Preliminary Results of an Extraordinary Mountain Wave Event over the Pyrenees during ALPEX.

Thomas A. Hafner, Yale University, USA
Presented at the XVIII. OSTIV Congress, Hobbs, USA (1983)

Summary

The observations of an extraordinary mountain wave event over the Pyrenees are examined in order to study the mesoscale structure, the vertical flux of horizontal momentum and the dynamics of mountain induced, internal gravity waves. The aircraft observations are conducted during the Special Observation Period (SOP) of the Alpine Experiment (ALPEX) on March 23, 1982, in traverse flights across the Pyrenees, covering the troposphere and the lower stratosphere with the high instrumented aircraft platforms P-3 from NOAA and the Falcon - jet from the DFVLR.
Preliminary results of this case study include a description of the synoptic evolution and upstream conditions,
a presentation of the time series of the meteorological parameters along the flight traverses,
some comments on orographic forcing and two-dimensionality of the wave pattern,
an analysis of the fine structure of waves and turbulence patches, and, with special emphasis,
a comparison of the observed momentum flux profile to the predicted wave drag from linear theory.

1. Introduction

One of the major objectives of ALPEX is to study the mountain drag exerted from a mountain complex upon the atmosphere. Following the recommendations of Lilly (1972), special attention should be given to the wave drag, which is the vertical transport of horizontal momentum in mountain waves, and its variations with height for different types of waves and for various upstream conditions of the synoptic flow field.
Mountain wave observations which enable a detailed description of the mesoscale flow structure as well as a computation of the momentum flux require high standard aircraft measurements with a high degree of accuracy. Only few of the numerous mountain wave observations (Smith, 1979, supplies a long but still incomplete list) meet this requirement. Most of the applicable studies were conducted in areas of large scale mountain ranges, such as the Sierra Nevada and the Front Ranges of the Rocky Mountains, whereas sophisticated observations in medium-scale mountains like the Alps or the Pyrenees are still missing. ALPEX was determined to provide these data. Unfortunately, no classical deep South Foehn event with extensive mountain waves occured during the SOP of ALPEX. However, during the period of March 21 - 23, a perpendicular and strong airflow persisted across the Pyrenees and produced an extraordinary mountain wave event and foehn effects south of the Pyrenees. In a joint flight mission, P-3 from NOAA and the Falcon - jet from the DFVLR were sent out to gather meteorological data along a box flight pattern over the Pyrenees at different altitudes up to 13000 m with the special purpose to examine the degree of the two-dimensionality of mountain waves.
The Pyrenees are a medium-size mountain range with a length of about 380 km, a mean width of about 80 km, a mean barrier height of 2400 m and a maximum height of 3404 m of the Pico de Aneto. The Pyrenees connect the Atlantic Ocean and the Mediterranean Sea in an almost straight line seperating France from Spain.
A first analysis of the quick look data was performed by Hafner (1982) shortly after the observations. Although, these data were not quality proved and the analysis was done by hand, it showed clearly that the gathered data are useful to fill the observational gap concerning mountain waves of medium scale mountains.
The advanced analysis of the present paper highlights the mesoscale structure of the mountain waves and the amount and vertical distribution of wave momentum flux. Furthermore, the applicability of linear mountain wave theory on wave drag and the assumption of a two-dimensional flow field are examined. However, the present stage of the analysis is still incomplete and should be treated as preliminary results.

2. Synoptic evolution and upwind conditions.

On March 21, a lee cyclone forms in the Ligurian Sea south of Genoa. Combined with the high pressure area over the Eastern Atlantic, a surface pressure difference of more than 32 hPa promotes a strong northerly flow of cold and moist air towards the Pyrenees which extends vertically up into a northerly jetstream with windspeeds up to 120 kn. The Scorer Parameter l^2 (z) computed from the upwind sounding of Toulouse at 12 GMT decreases rapidly between 700 and 600 hPa, and thus satisfies Scorer's condition for the occurrence of trapped lee waves. The satellite image (Fig. 1) exhibits the characteristics of the incoming blocked flow over France as well as a remarkable train of trapped lee waves south of the Pyrenees, penetrating more than 350 km into Spain and starting again behind the coastal mountains of the Massif de l'Ouarsenis in Algeria. The visible part of the wave pattern consists of wave-ripples of about 8.5 km wavelength.
During March 22, there are no dramatical changes of the synoptic fields and the lee wave activity, although the jetstream slows down to about 80 kn and the lenticularis clouds vanish, because subsidence leads to the dry-out of the leeside airmasses.
On March 23, the surface low has moved to the Ionian Sea, the high pressure area has strengthened and is now centered over England. This surface pressure configuration (Fig. 2) leads to a shallow north-northeasterly flow of cold and moist air towards the Pyrenees. The geopotential distribution shown on the upper charts confirm a persistent northerly flow across the Pyrenees with windspeeds of 45 kn at 700 hPa (Fig. 3). The analysis of the isotachs in Fig. 4 shows that a broad northerly jet-stream band remains fully developed at 300 hPa with maxwinds of more than 100 kn above the eastern part of the Pyrenees. The satellite image (Fig. 5) summarizes all of the ALPEX-relevant phenomena of March 23, such as excellent Bora conditions in Yugoslavia, shallow north-foehn in the Po-valley, weakening mistral in the lower Rhône-valley, and some details of an extraordinary north-foehn event near the Pyrenees, especially featuring the blocked shallow stratocumulus layer on the upwind-side, the sharp border of the foehn-clearing and cirrostratus clouds on the lee-side, which indicate the presence of a deep mountain wave system.
The upstream conditions (Fig. 6a, b) of the wind- and temperature field, and the characteristic profiles of the Gradient Richardson number Ri, the Scorer parameter l^2, and the Brunt-Väisälä frequency N are derived from the rawinsonde data of Toulouse (12 GMT);

$$Ri = \frac{g\,\Theta_z}{\Theta\,U_z^2} = \frac{N^2}{U_z^2} \quad - (1)$$

$$l^2 = (N/U)^2 - U_{zz}/U \quad (2)$$

It is expected from the synoptic evolution, the satellite image and from the upwind conditions that mountain waves and foehn effects appear south of the Pyrenees.

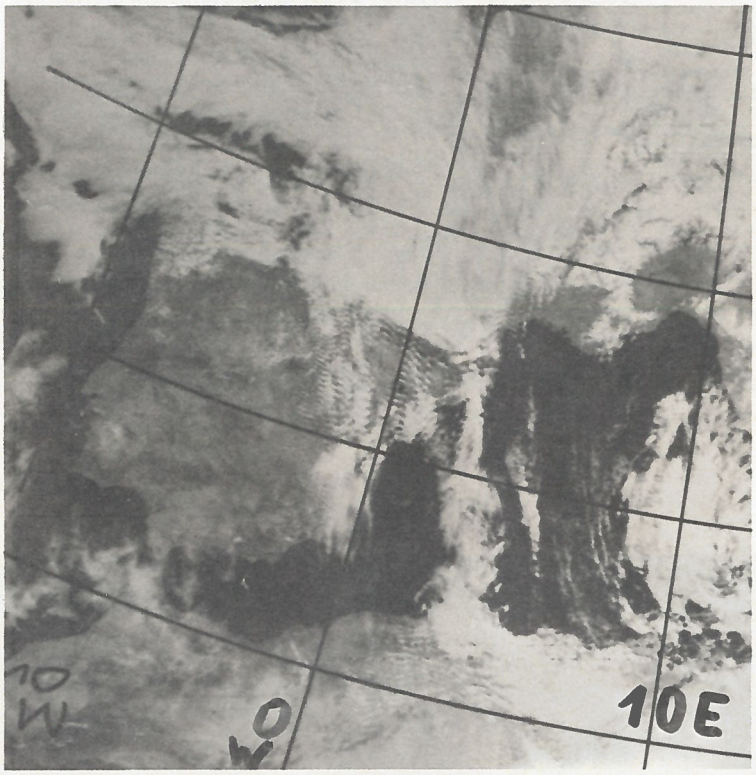

Fig. 1: Satellite image NOAA 7 VIS from March, 21, 1982 (13.44 GMT).

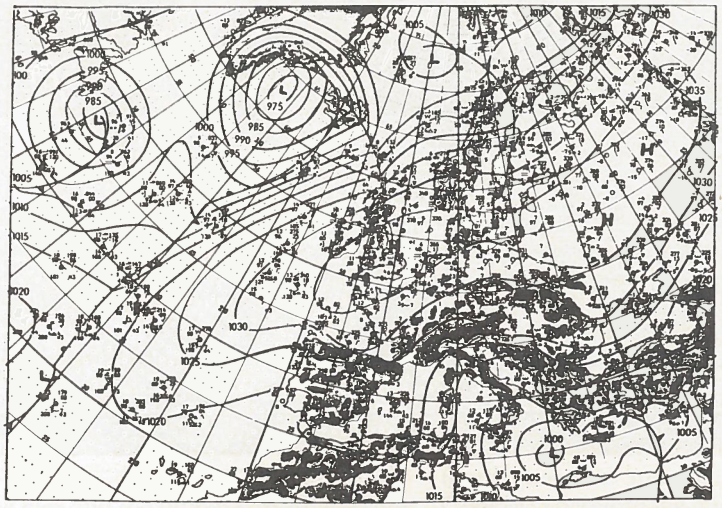

Fig. 2: Surface weather chart from March 23, 1982 (12 GMT), from DWD.

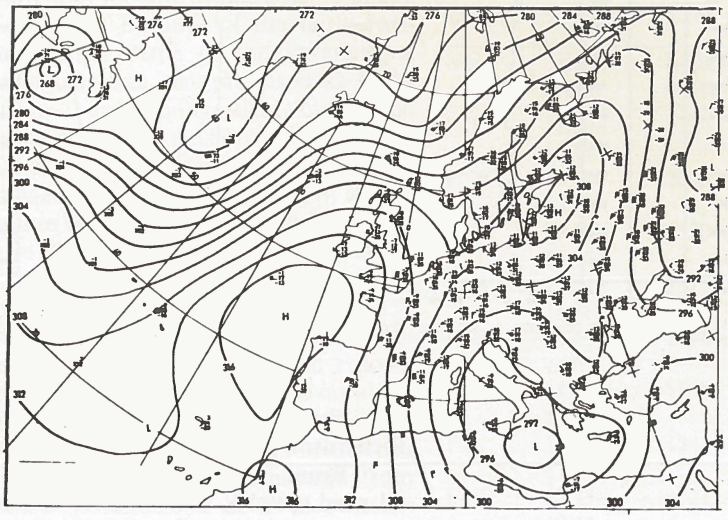

Fig. 3: 700 hPa chart from March 23, 1982 (00 GMT), from DWD.

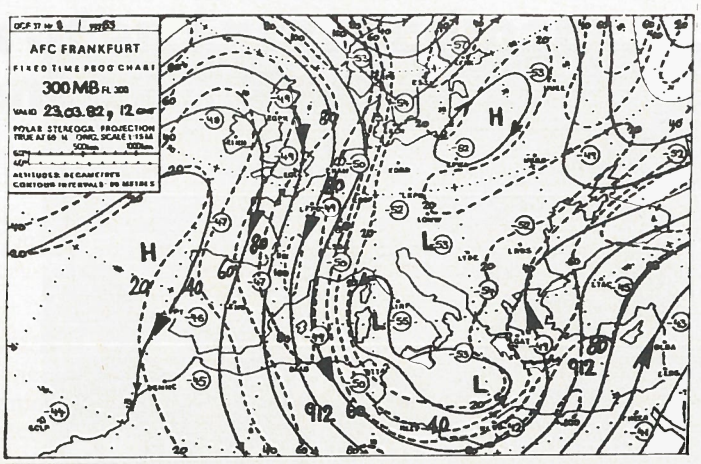

Fig. 4: 300 hPa chart from March 23, 1982 (12 GMT) with isohypses in gpdm, isotachs in kt (dashed) and temperatures in °C (circles), from DWD.

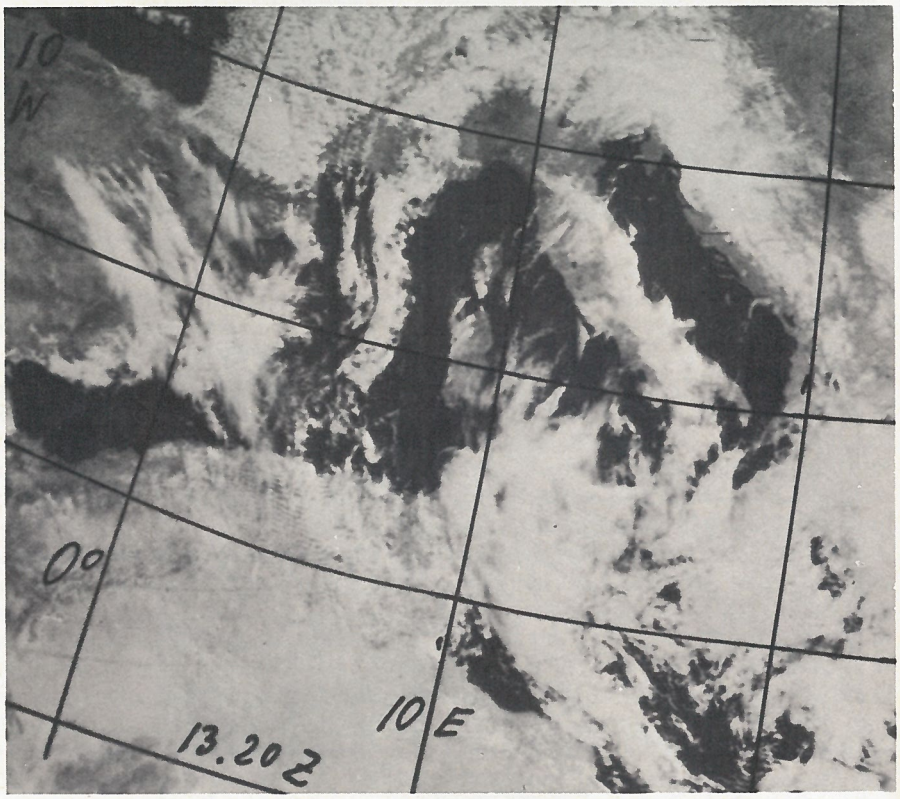

Fig. 5: Satellite image NOAA 7 VIS from March 23, 1982 (13.20 GMT).

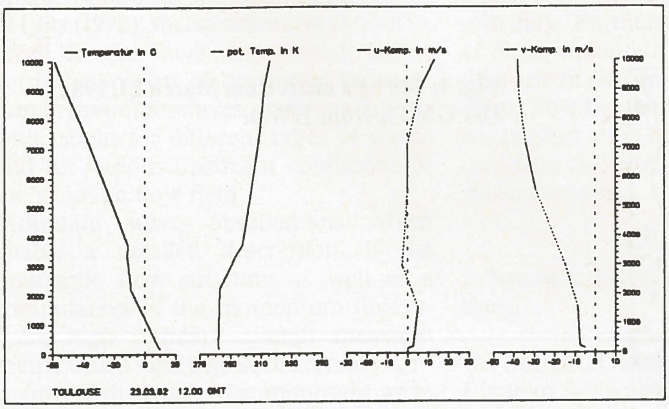

Fig. 6a: Wind and temperature sounding of Toulouse from March 23 (12 GMT).

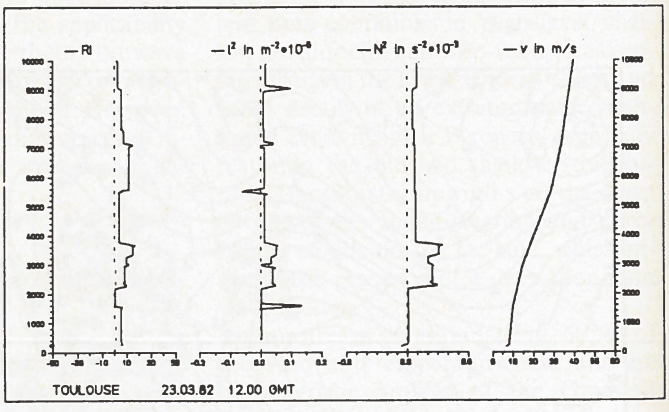

Fig. 6b: Vertical profiles of Gradient Richardson Number Ri, Scorer Parameter l^2, Brunt - Väisälä frequency N and total wind speed V, derived from Toulouse sounding from March 23 (12 GMT).

3. Platforms, mission planning and data.

Most of the data for this study are provided from the ALPEX aircraft platforms P-3 and Falcon. P-3 is a four-engine turboprop aircraft owned and operated by the National Oceanic and Atmospheric Administration (NOAA) of the United States Department of Commerce. With a range of 3600 nm and an endurance of almost 12 hours, it is suitable for long range missions in the lower and middle troposphere. The Falcon is a light two-engine jet-aircraft which is owned and operated by the Deutsche Forschungs- und Versuchsanstalt für Luft- und Raumfahrt (DFVLR). Fully equipped it has a range of only 1150 nm, but it is able to make measurements in the higher troposphere and lower stratosphere up to about 41000 ft. During the Special Observing Period (SOP) of ALPEX, both aircraft were operating from the ALPEX Operation Center (AOC) in Geneva, Switzerland.
The accuracy and resolution of the relevant aircraft instrumentation for this study are briefly summarized in Table 1. For detailed information about the instrumentation of the ALPEX aircraft, the 'ALPEX Aircraft Atlas', edited by P. J. Kennedy (1982), is recommended.

Table 1: Accuracy and resolution of the instrumentation of Falcon and P-3.

Parameter	Accuracy	Resolution
wind u,v	1.5 ms^{-1}	0.1 ms^{-1}
	(1.0 ms^{-1})	0.05 ms^{-1})
	1.5 ms^{-1}	0.1 ms^{-1}
	(0.5 ms^{-1})	(0.01 ms^{-1})
temperature	0.2 K	0.05 K
	(0.2 K)	(0.03 K)
static pressure	0.25 hPa	0.25 hPa
	(0.2 hPa)	(0.04 hPa)
altitude	1 m	0.5 m
	(1 m)	(0.1 m)
geographical coordinates	depends on flight time	0.5″
	(0.02°)	(0.003″)

The idea and the proposal of a flight mission from Geneva all the way down to the Pyrenees was brought up by Ronald B. Smith after looking at the satellite image of Figure 1. Because of the fairly two-dimensional shape of the Pyrenees, a rectangular box was proposed as flight pattern in order to investigate mainly the degree of two-dimensionality of the airflow and the wave pattern.
On March 22, the first attempt of a joint mission of Falcon and Electra failed, because Electra had an engine failure already over France, and the Falcon didn't get permission to enter Spanish airspace.
On March 23, a second attempt was successfully performed by P-3 and Falcon. Both aircraft completed two boxes along the actual flight tracks shown in Fig. 7. The crossmountain traverses of the box run almost exactly northsouth from Gaillac to Barcelona at 2° E (eastern traverse) and from Reus to Agen at 1° E

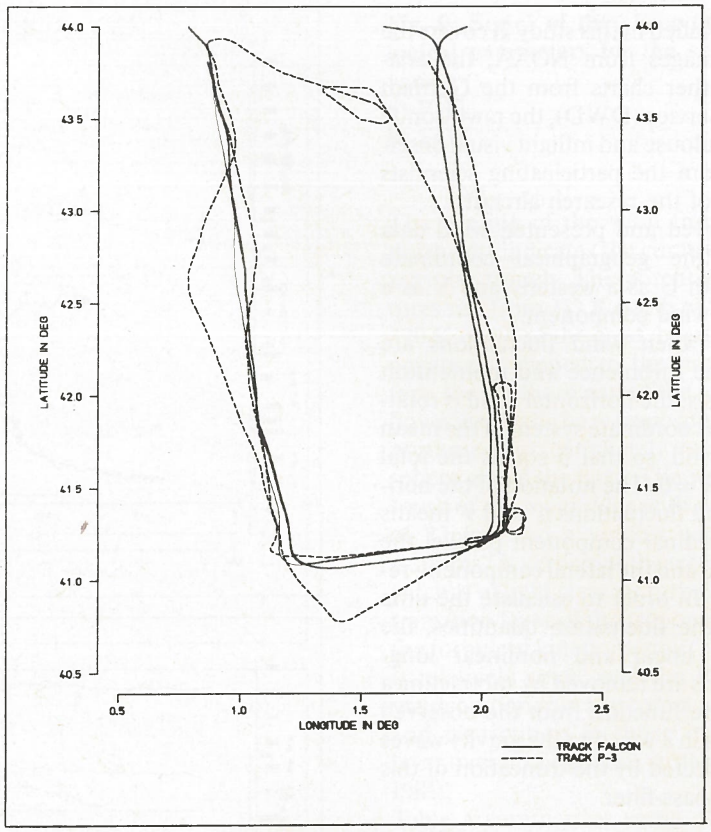

Fig. 7: Flight track of Falcon and P-3 (dashed line) inside the box pattern across the Pyrenees.

(western traverse); they are separated by a mean distance of about 90 km. The vertical displacement and other details from the traverse flights are listed in Table 2. After the first and second traverses, the P-3 performed aircraft soundings down to Barcelona and Toulouse; after the third traverse 2 drop-wind sondes were released. Originally, a third box was planned for P-3 to cover the intermediate flight levels 250 and 280. Unfortunately, P-3 lost thrust on one engine at the end of the fourth traverse and had to return to Geneva. Therefore the intermediate data which should connect the lower boxes of the P-3 with the high-level boxes of the Falcon got lost. The Falcon had to make an intermediate landing between the two boxes to get refueled in Bordeaux. For these reasons, the temporal synchronization of the aircraft is poor and the flights along the same traverses differ remarkably in time (see Table 2). This fact should be kept in mind whenever the steady state assumption has to be used in the analysis. In addition to the officially released ALPEX 1 Hz-aircraft data set, information from the so called 'Quick Look Data

Table 2: Traverses of Falcon (F) and P-3 (P); (E-eastern, W-western traverses).

No.	Times GMT	Length in sec	Flight-level	Heading	Remarks
P1E	12.50–13.19	1790	130	S	Followed by a descent to Barcelona
P2W	14.14–14.58	2600	140	N	Followed by a descent to Toulouse
P3E	15.19–15.45	1530	190	S	Followed by the release of 2 drop-wind sondes
P4W	15.54–16.46	3077	180	N	one engine lost at the end of the traverse
F1E	13.43–14.03	1178	370	S	
F2W	14.11–14.40	1700	390	N	Followed by a landing in Bordeaux
F3E	17.16–17.37	1241	330	S	
F4W	17.45–18.14	1727	310	N	

Sets' is included in this study. It covers the satellite images from NOAA, the analyzed weather charts from the German Weather Service (DWD), the rawinsonde data of Toulouse and inflight visual observations from the participating scientists on board of the research aircraft.

The observed and presented wind data refer to the geographical coordinate system with U as a westerly and V as a southerly wind component.

However, when wind fluctuations are used in the turbulence and momentum flux analysis, the horizontal wind is rotated into the coordinate system of the mean traverse wind, so that $\bar{u}$ equals the total wind and $\bar{v} = 0$. The notation of the horizontal wind fluctuations u' and v' means the longitudinal component parallel the mean wind and the lateral component, respectively. In order to calculate the time series of the fluctuation quantities, the unwanted linear and nonlinear longwave trends are removed by subtracting a cubic spline function from the observed time series in a way that the gravity waves are not affected by the truncation of this weak highpass-filter.

4. Results

4.1. Time series of the meteorological parameters.

The observed series of the meteorological variables along the flight traverses are plotted versus latitude. This simplifies the comparison of the up- and downwind directed traverses from Falcon and P-3, because the series become independent of the ground speed; it also allows direct estimates of the horizontal wavelengths. Fig. 8a and b summarize the potential temperatures along the eastern and western traverses above the appertaining cross-sectional profiles of the Pyrenees. The variations of the potential temperatures indicate a phase reversed wave motion. These undulations are particularly pronounced in the Falcon-levels near the tropopause due to the stable stratification, whereas they do not show up so clearly in the lower P-3 levels. In both sections the primary mountain wave is located above the slope on the leeside of the mountain ridge. The vertical phase lines are tilted into the mean wind and indicate an upward propagating energy flux and the associated downward directed flux of horizontal momentum, which is discussed in Chapter 4.4.

In the higher levels the wave pattern is almost consistent and two-dimensional, because it depends mainly on the tuning state of the atmosphere. In the lower levels, where the wave is generated, orographic and convective forcing play a dominant role in the structure of the wave field. Since the orography is not completely two-dimensional, a two-dimensional response cannot be expected.

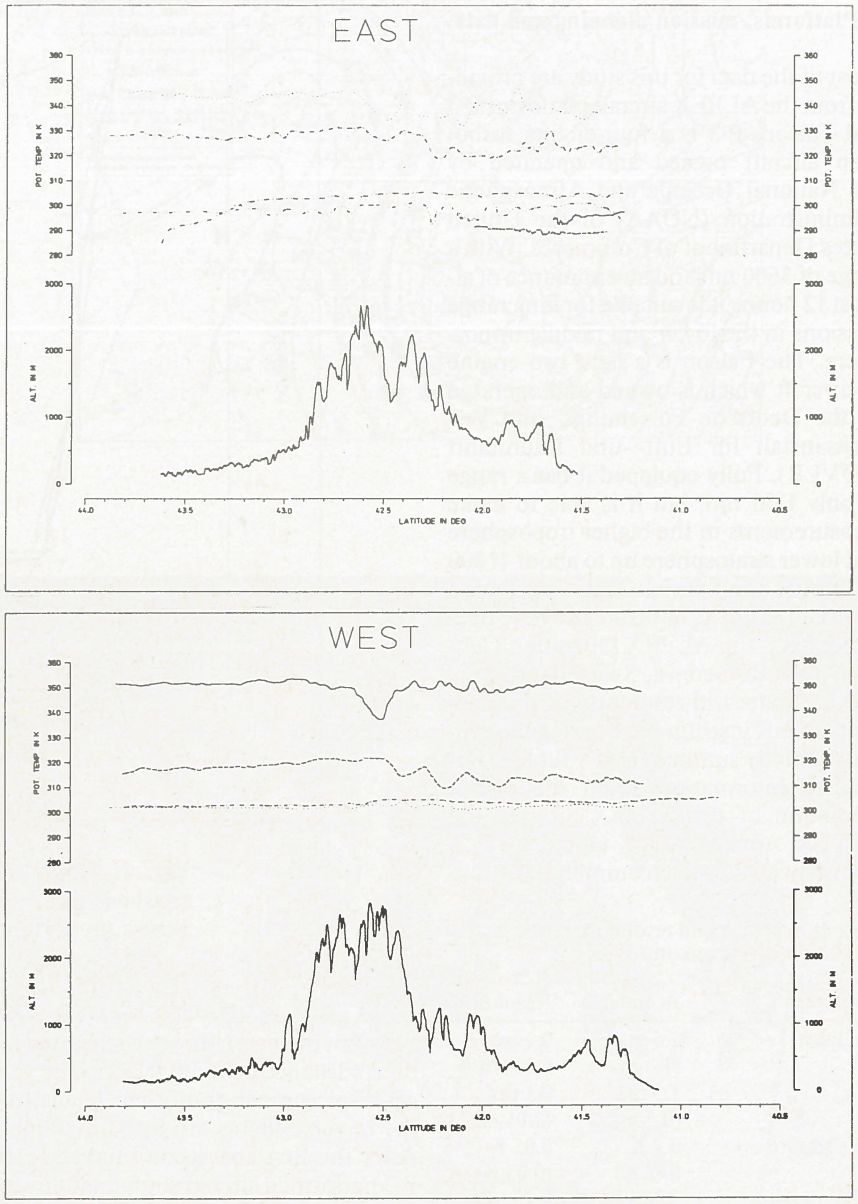

Fig. 8: Series of potential temperature of all flight traverses.
a) above the eastern profile,
b) above the western profile.

Spectral analysis of the orographic profiles from radar altimeter data is performed and compared with that of the w-component for the P-3 levels. The maximum wavelengths of the orography λ_{oro} and the w-wave response λ_w are given in Table 3 (with the secondary maxima in brackets). The traverses with good agreement of these wavelengths include trains of 5–7 smooth waves with resonance properties.

In addition, the forcing caused by convective elements and the interaction of the waves with the boundary layer modify the flow field on different time scales, so that the wave response has to be treated as a transient process which contradicts the steady state assumption of linear wave theory. Taking also into account a time lag of 2.5 hours and 2.0 hours between the lower traverse flights along the eastern and western section, respectively, it is not surprising that at least the lower wave pattern seems to be incoherent.

Table 3: Wavelengths of orography and w-waves.

No.	λ w	λ oro
P1E	8.0 (15.5)	15.0 (35.0)
P2W	19.2 (5.7)	29.8 (10.8)
P3E	29.0 (5.8)	24.8 (5.8)
P4W	31.0 (10.6)	28.0 (10.6)

In Fig. 9a and b two selected series of the observed meteorological parameters are shown for the individual traverses P1E and F4W above the corresponding orographic profiles (see also Table 4).

The first and lowest traverse (P1E) approaches the Pyrenees in FL 130 from the north above a strato-cumulus cloudlayer. Upstream of the Pyrenees small amplitude waves ($w = \pm 1.5$ ms^{-1}) with wavelengths of about 13 km are encountered. On the leeside of the main ridge the potential temperature drops by almost 10 K and a wave train starts, including 6–7 waves with decaying amplitudes downs-

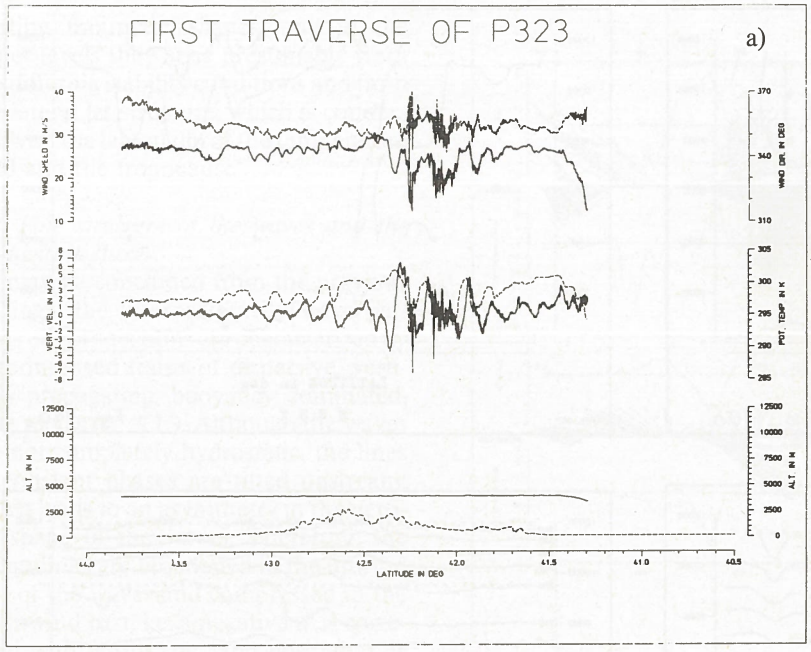

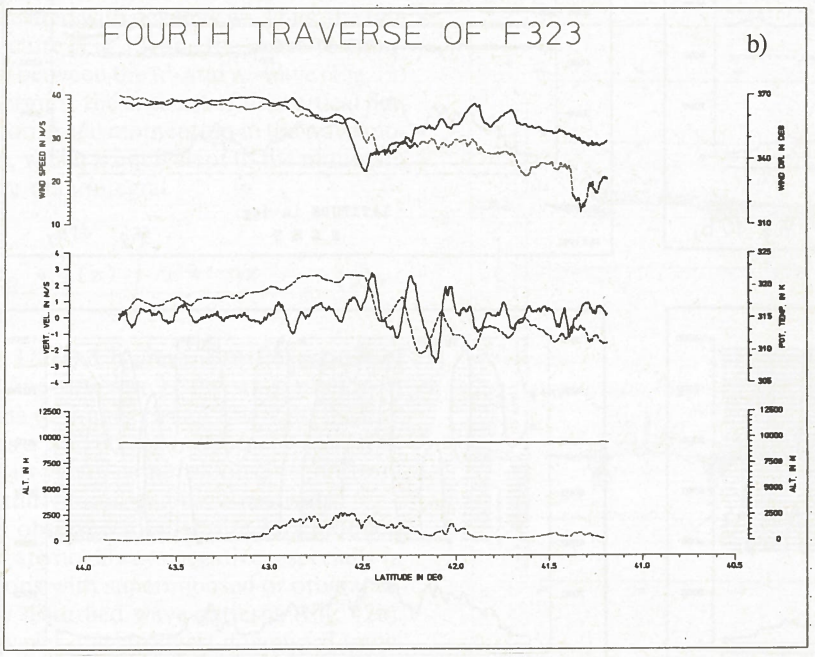

Fig. 9: Series of the observed meteorological parameters for the selected traverses,
a) P1E,
b) F4W.

Table 4: Observed wind, turbulence characteristics and wavelengths deduced from the time series.

No.	$\bar{U}$ ms^{-1}	$\bar{V}$ ms^{-1}	A1	A2	A3	TKE	λ km	Remarks
P1E	2	-25	2.84	1.77	2.43	5.70	22	incl. mod. lee turb.
P2W	-2	-31	2.24	2.03	2.45	5.05	18	smooth wave
P3E	4	-35	3.86	3.12	2.77	10.77	24	persistent waves
P4W	1	-36	2.31	1.81	1.48	3.60	24	light smooth waves
F1E	11	-27	2.16	2.19	1.01	3.49	25	smooth long waves
F2W	12	-27	4.57	5.45	1.89	18.05	32	incl. shorter waves and
F3W	3	-27	4.73	2.30	2.32	11.02	30	light turbulence
F4W	4	-33	2.65	2.13	1.53	4.63	23	light waves, only little turbulence

tream. The huge primary mountain wave has a wavelength of about 22 km and the highest vertical windspeed of all traverses with +5.5 ms^{-1}. In the following first wave trough a rotor produces a downcraft with w = -8.2 ms^{-1} and light turbulence. The second wave indicates overturning on the top, following by a region of moderate turbulence, which is also visible in the wind data. Except for the two small turbulent regions the air motion in- and outside of the waves is very smooth and quasi-laminar. The turbulent kinetic energy (TKE) is therefore small and includes a relatively large contribution from the standard deviation of the vertical wind component (A3) from the wave motion.

The second traverse, which is discussed in greater detail, is the last Falcon-traverse F4W, which was flown from south to north above the western profile at FL 310.

The veering of the wind from north to northwest indicates the curative of the jet into the trough. The potential temperatures rise from 312 K south of the crest to 320 K north of the crest, because the tropopause is dipped to the north. Therefore, the southern part of the traverse was flown inside the hazy troposphere and the northern part completely in the stratosphere above the haze. The wave motion south of the main ridge with wavelengths of 23 km and a vertical windspeed of ± 2.5 ms^{-1} is very smooth, except for some patches of light clear air turbulence in the transition layer of the tropopause. Again, the turbulent kinetic energy (TKE = 4.63) is relatively small, and the RMS of the windcomponents are comparable in size and distribution to those in a Prandtl-layer over homogenous surfaces (Hafner, 1981).

Table 4 summarizes some of the mean and turbulence characteristics of the flight traverses. $\bar{U}$ and $\bar{V}$ are the mean westerly and southerly wind components. A1, A2 and A3 are the normalized standard deviations (RMS) of the longitudinal, lateral and vertical wind fluctuation components

$$A1 = (\overline{uu} / u_{*1}^2)^{1/2}$$
$$A2 = (\overline{vv} / u_{*1}^2)^{1/2} \qquad (3a\text{-}c)$$
$$A3 = (\overline{ww} / u_{*1}^2)^{1/2}$$

with a local friction velocity

$$u_{*1}^2 = (\overline{uw}^2 + \overline{vw}^2)^{1/2} \qquad (3d).$$

The turbulent kinetic energy is defined as

$$TKE = \frac{1}{3}(A1^2 + A2^2 + A3^2) \qquad (4),$$

and λ is the mean wavelength of the gravity waves.

4.2. Mesoscale cross-sectional analysis.

Despite the previously described limitations of the aircraft data, objective cross-sectional analysis was performed for the eastern (Fig. 10) and western cross-sections (Fig. 11) in order to describe the details of the mesoscale temperature and flow field and to visualize its lateral deviations due to the three-dimensional flow characteristics.

In both sections, the temperature- and wind-fields are well correlated, and no clouds were observed along the flight legs. This justifies the assumption of steady state and adiabatic motion, and thus the isentropes can be interpreted as streamlines.

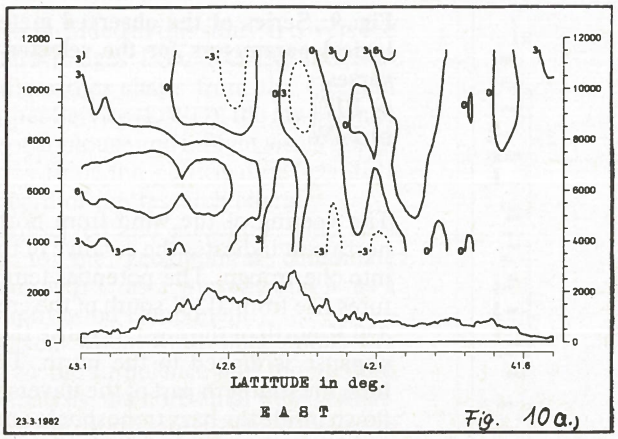

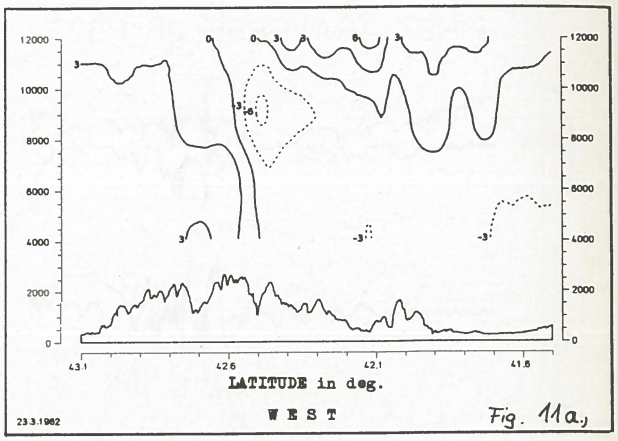

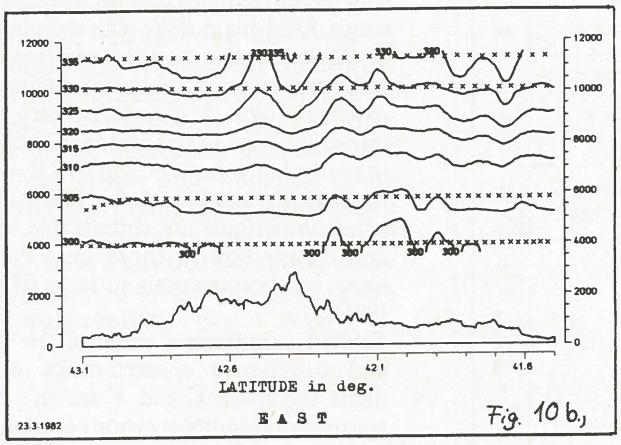

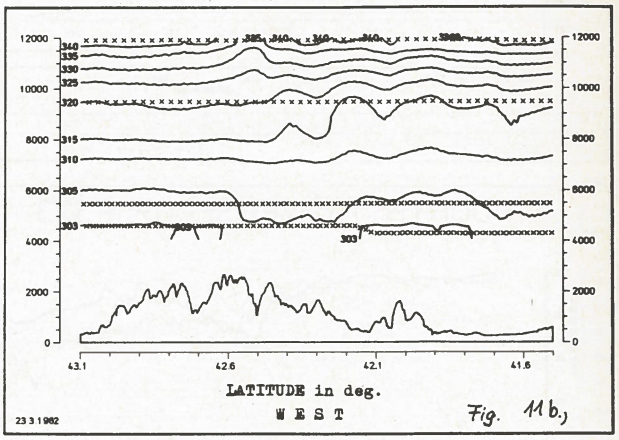

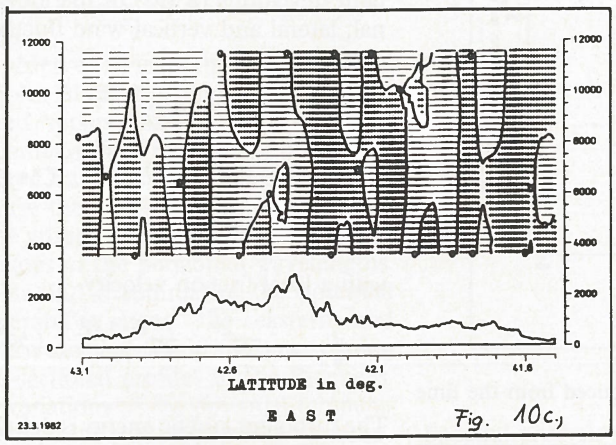

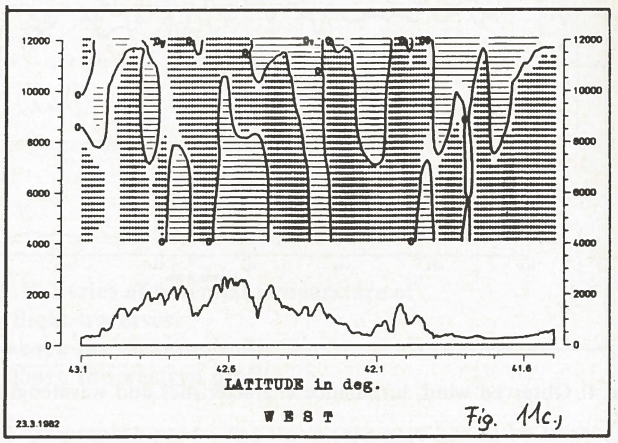

Fig. 10: Eastern cross-section analysis of
a) isentropes with flight paths (xxx)
b) isotachs of longidudional wind fluctuations,
c) vertical wind (+ upward, - downward, extra bold - strong).

Fig. 11: As fig. 10, except for the western cross-section.

The prominent features of the airflow behaved similarily in both sections: Upstream of the mountains the flow was accelerated and ran into a stationary, vertically propagating train of mountain waves, which decayed rapidly to the south. The primary waves were accompanied by minima of the horizontal wind speed at a height of about 9000 m and maxima of the vertical wind speed in the lower levels. In the temperature field, however, the amplitudes and the consistency of the wave patterns were much higher in the upper levels. On the leeside, a general destabilization of the midtroposphere was observed and connected to the cooling of the upper air and the heating of the lower troposphere due to the subsiding foehn air. The low level blocking of cold air on the windward side of the Pyrenees happened below the lowest flight traverse, and therefore it is not shown in the cross-sections.

Besides the obvious similarities there are also distinct differences in the analyzed fields of the crosssections. In the eastern section the wave pattern is more pronounced and coherent and the wave amplitudes are larger. The differences in the lower levels are caused by the con-

trasting mountain shapes, and in the upper levels they arise presumably from the differing stability conditions and from the lateral jet structure, which is connected with the lateral dip of the temperature field and the tropopause.

4.3. Fine structure of the waves and the momentum fluxes.

As may be concluded from the previous findings, the internal gravity wave patterns of both sections are characterized by superimposed trains of dispersive, vertically propagating, buoyancy dominated, long waves ($k^2 \ll l^2$). Although the waves are not completely hydrostatic, the lines of constant phases are tilted upstream, which leads to an asymmetry in the vertical shape of the waves. Therefore, the streamlines are broadened in the upwind part of the waves and compressed in the downwind part, i.e. a negative u' is correlated with positive w', and positive u' is correlated with negative w'. Thus, the fine structure (Fig. 12) and the phase-relationship between the u'- and w'-wave (Fig. 13) determine the amount of the vertical flux of horizontal momentum in the wave motion, which is equivalent to the mountain wave drag integral

$$D_2 = \varrho(z) \int_{-\infty}^{\infty} u'w' \, dx \qquad (5).$$

Fig. 12a and b present two examples of the fine-structure of the wave motion in terms of time series of the wind fluctuations u' and w', the products u'v' and u'w' and its vector compositions in a horizontal and vertical plane, respectively.

The observed momentum flux products u'w' are not always negative, especially in regions with superimposed or orographically disturbed wave patterns (Fig. 12b). However, the strongest downward transport of momentum occurs usually in the downwind part of the waves with positive u' and negative w'.

Another qualitative measure of the direction of momentum fluxes is the phase relationship between the u' and w'-waves. Independent of the leading variable there is a maximum of downward momentum flux for a phase angle $\varphi = 180°$ and a maximum of upward momentum flux, if both waves are in phase. No momentum flux contribution is expected if the phase angle equals 90° or 270°. This relationship is illustrated by the phase circle in Fig. 13. Here, φ is defined so that the w'-wave leads the u'-wave. In addition, Fig. 13 contains the phase angles φ of all waves observed. They are clustered between 90° and 145° indicating a slight but general downward directed momentum flux.

In Fig. 12, the conspicuous feature of the large and meandering u'v'-vectors deserve further consideration. They confirm either that the wave patterns are threedimensional to a higher degree than expected or that the mean flow is not

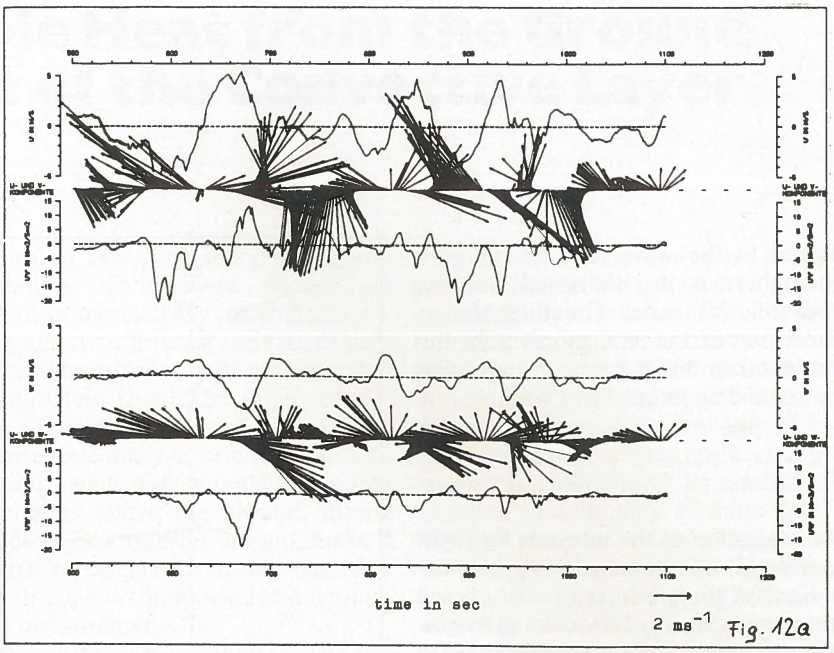

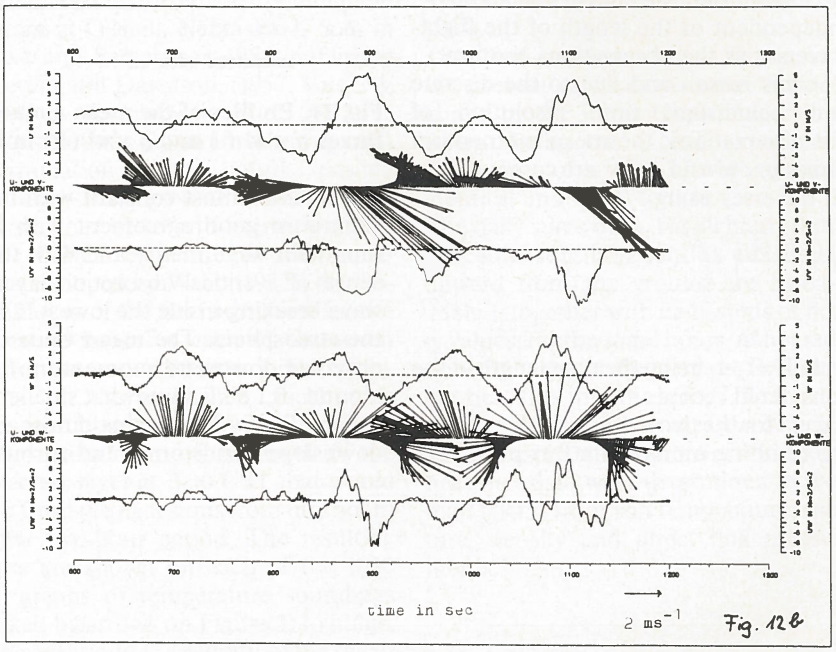

Fig. 12: Time series of wind fluctuations u' and w', fluctuation products u'v' and u'w' and its vector presentation for the selected traverses
a) F1E,
b) P3E.

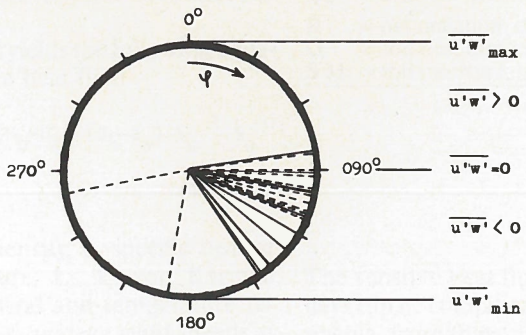

Fig. 13: Momentum flux u'w' related to phase angle φ between w' and u' of all observed waves from the Falcon traverses (——) and the P-3 traverses (---).

aligned to the wave patterns, or both, since there is no horizontal restoring force on this scale. The three-dimensional part or the total momentum flux can be taken into account by expanding the wave drag integral in (5) to

$$D_3 = \varrho(z) \int_{-\infty}^{\infty} u'w'\,dx + \varrho(z) \int_{-\infty}^{\infty} v'w'\,dx \quad (6).$$

The evaluation of the integrals for flight traverses with finite lengths is problematic because the products of u'w' exceed the integral value by 1-2 orders of magnitude, and there is always a contribution to the momentum flux above real surfaces independent of the length of the flight-traverses as the observations confirm.
For this reason and due to the discrete and equidistant time resolution of the observations, the mean momentum fluxes ϱ u'w' and ϱ v'w' are computed for all traverses using

$$D_3 = \frac{\varrho(z)}{T} \left\{ \int_{t_1}^{t_2} u'w'\,dt + \int_{t_1}^{t_2} v'w'\,dt \right\} \quad (7)$$

with $T = t_2 - t_1$ being the time length of the considered record.
Except for the two traverses P1E and F1E, the resulting momentum flux profiles of

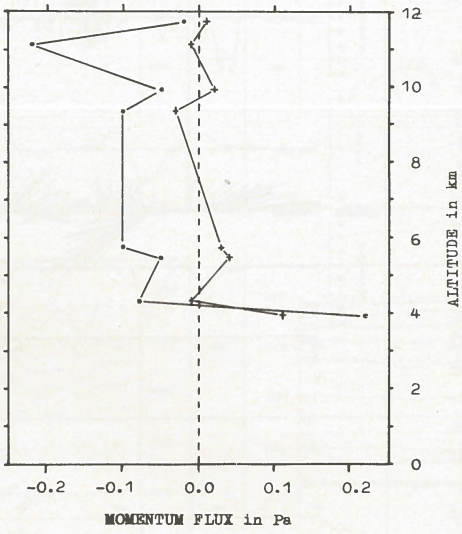

Fig. 14: Profiles of the mean momentum fluxes ϱ u'w' (·) and ϱ v'w' (+) in Pa.

Fig. 14 are almost constant with height. This is in good agreement with linear mountain wave theory and with the absence of a critical absorption layer and wave breaking inside the lowest 12 km of the atmosphere. The mean value of the observed downward momentum flux of around -0.1 Pa is somewhat smaller than for the Rocky Mountains during severe downslope windstorms and turbulence, for which linear theory is not applicable. Lilly and Kennedy (1973) report a mean value of -0.7 Pa and Lilly (1978) –1.2 Pa for an extraordinary strong event. Nevertheless, the wave drag of a smooth airflow over a medium-scale mountain range like the Pyrenees has a strong impact on the atmospheric flow, and it is at least of equal importance has the drug due to surface friction.

5. References

Hafner T.A. (1981): Turbulenzstrukturen in der atmosphärischen Grenzschicht abgeleitet aus den Varianzen der Windgeschwindigkeitskomponenten, Dipl.-arbeit, Universität Karlsruhe.
Hafner, T.A. (1982): Leewaves over the Pyrenees, in 'ALPEX Preliminary Scientific Results' (ed. J.P. Kuettner), GARP-ALPEX No. 7, 218-226, WMO, Geneva.
Kennedy P.J. (1982): An ALPEX Aircraft Atlas, NCAR, Boulder.
Lilly D.K. (1972): Wave momentum flux - a GARP problem, Bull. Am. Met. Soc. 53, 17-23.
Lilly D.K. (1978): A severe downslope windstorm and aircraft turbulence event induced by a mountain wave, J. Atmos. Sci., 35, 59-77.
Lilly D.K. and *P.J. Kennedy* (1973): Observations of a stationary mountain wave and its associated momentum flux and energy dissipation, J. Atmos. Sci., 30, 1135-1152.
Smith R.B. (1979): The influence of mountains on the atmosphere, Advances in Geophysics, 21, 87-230.